第 31卷 第 1期　　焊　接　学　报　　Vol.31　No.1
2010年 1月　　TRANSACTIONS OF THE CHINA WELDING INSTITUTION　　January　2010

近似熵与熔滴过渡频率对表征 CO_2焊短路过渡过程稳定性的不同影响

向远鹏[1]，　曹　彪[2]
（1. 电子科技大学 机械电子工程学院，成都　611731；
2. 华南理工大学 机械与汽车工程学院，广州　510641）

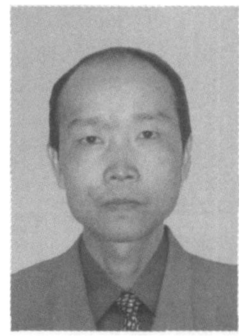
向远鹏

摘　要：基于不同电弧电压、气体流量、焊接速度下短路过渡 CO_2焊的焊接电流时间序列，利用 Pincus算法，评估了焊接电流的近似熵，分析了近似熵与熔滴过渡频率对表征焊接过程稳定性的不同影响．试验与数值分析证明在上述三种工艺条件下近似熵越大，焊接过程的稳定程度越高，然而熔滴过渡频率与焊接过程的稳定性变化趋势难以取得一致，因此焊接电流近似熵比熔滴短路过渡频率更为准确地刻画了焊接过程稳定性的动态变化，用于定量表征焊接系统的稳定性时优于熔滴过渡频率．

关键词：CO_2；熔化极气体保护电弧焊；近似熵；熔滴过渡频率
中图分类号：TG115.28　文献标识码：A　文章编号：0253－360X（2010）01－0021－04

0　序　　言

20世纪 90年代初，Pincus从量化时间序列复杂性的角度提出并发展了非线性统计量近似熵 A_E的概念[1,2]，此后许多学者在物理、化学、电子、机械和经济等领域利用近似熵来分析采样时间序列，并取得了令人满意的效果．计算近似熵所需的数据量较小，对时间序列中存在的少量异常数据不敏感，而且适用于确定性信号和随机信号[2]．

CO_2短路过渡焊接时，为了稳定焊接过程，总是希望熔滴越小、过渡越快越好，也就是说，要求尽量高的短路过渡频率，因此传统生产实践中常常将熔滴短路过渡频率作为衡量短路过渡过程是否稳定的标准[3]．

文中将深入探讨不同工艺条件下焊接电流近似熵与 CO_2焊短路过渡过程稳定性的定量关系，并与熔滴短路过渡频率作一系统分析与比较．

1　算　　法

近似熵刻画了时间序列的复杂性，以下是它的确切定义[1,2]．

将长度为 N的时间序列 $\{u(i)\}$按照顺序组成 m维矢量 $X(i)$，即

$$X(i)=[u(i),\ u(i+1),\ \cdots,\ u(i+m-1)]$$
$$i=1,2,\cdots,N-m+1 \tag{1}$$

对于每一个 i值计算矢量 $X(i)$与其余矢量 $X(j)$之间的距离，取极大值范数，即

$$d[X(i),X(j)]=\max_{k=0\sim m-1}|u(i+k)-u(j+k)| \tag{2}$$

给定相似容限 $r(r>0)$，对于每一个 i值统计 $d[X(i),X(j)]<r$的数目以及该值与总的矢量数目 $N-m+1$的比值，记为 $C_i^m(r)$，即

$$C_i^m(r)=H(r-d[X(i),X(j)])/(N-m+1) \tag{3}$$

$H(\cdot)$为 Heaviside函数．先将 $C_i^m(r)$取对数，再求其对于所有 i的平均值，记为 $\Phi^m(r)$，即

$$\Phi^m(r)=\frac{1}{N-m+1}\sum_{i=1}^{N-m+1}\ln C_i^m(r) \tag{4}$$

再对 $m+1$，重复上述过程，从而得出 $\Phi^{m+1}(r)$．

定义近似熵为

$$A_E(m,r)=\Phi^m(r)-\Phi^{m+1}(r) \tag{5}$$

式中：m，r分别是比较向量模式维数和相似容限，通常取 $m=2$，$r=(0.10\sim0.25)SD(u)$，SD代表时间序列 u的标准差[2]．

2　试验方法

利用焊接电源 Fronius TPS2700，在 2.5 mm厚

收稿日期：2009－06－26
基金项目：国家自然科学基金资助项目（50375053，50575077）

低碳钢板(Q235)上进行短路过渡 CO_2 气体保护电弧焊平铺试验，填充材料为直径 ϕ1.0 mm的 H08Mn2SiA焊丝，保护气体为纯度 99.9%的 CO_2.

在分别改变电弧电压 U_a、气体流量 q和焊接速度 v_w的条件下进行了一系列工艺试验. 在每一组参数试验中，为了研究其对焊接过程稳定性和焊接电流近似熵 A_E 的影响，要保持其余 4个参数恒定不变，而将考察参数依次调节至一系列典型值. 焊接过程中借助 NI PCI-6221数据采集卡以 10 kHz采样率实时采样频焊接电流 50 s，从全部采样值中随机截取 $N=120\ 000$个数据点用于评估 A_E，基于每5000个点计算一个 A_E值，最后求取 24个近似熵均值 $\langle A_E\rangle$与其标准差 $\sigma(A_E)$，选取相似容限 $r=0.15SD(I_s)$，比较向量模式维数 $m=2$.

3 结果与分析

3.1 不同电弧电压 U_a下的近似熵 A_E分析

焊接工艺参数设定为：送丝速度 $v_f=4.0$ m/min，焊接速度 $v_w=30$ cm/min，气体流量 $q=10$ L/min，焊丝伸出长度 $l_e=8$ mm，依次改变电弧电压 U_a为 16，18，20，22，24和 26 V. 表 1列出了不同 U_a下近似熵均值 $\langle A_E\rangle$及标准差 $\sigma(A_E)$和熔滴过渡频率 f的最终计算结果，图 1a，b分别表明了 A_E随 U_a的变化和 U_a对于 A_E和 f的影响.

从试验过程可见，当 18 V≤U_a≤20 V时，焊接过程稳定均匀. 而当 U_a≤16 V时，焊接过程明显失稳，飞溅增加，这是因为 U_a太低时，弧长太短，焊丝末端与熔池之间的短路小桥不易破断，从而导致熔滴过渡周期中短路持续时间过长，燃弧时间太短，燃弧和短路期间的能量分配失衡， 降低.

表 1 不同电弧电压下近似熵均值及标准差和熔滴过渡频率

Table 1 Mean $\langle A_E\rangle$ and its standard deviation $\sigma(A_E)$ and droplet transfer frequency f at different arc voltages U_a

电弧电压 U_a/V	近似熵均值 $\langle A_E\rangle$	近似熵标准差 $\sigma(A_E)$	熔滴过渡频率 f/Hz
16	0.305 0	0.038 6	79
18	0.468 7	0.053 3	114
20	0.528 5	0.023 0	111
22	0.284 8	0.032 0	49
24	0.245 3	0.031 4	30
26	0.258 0	0.042 7	16

另外，短路小桥难于分离往往引起焊丝不规则

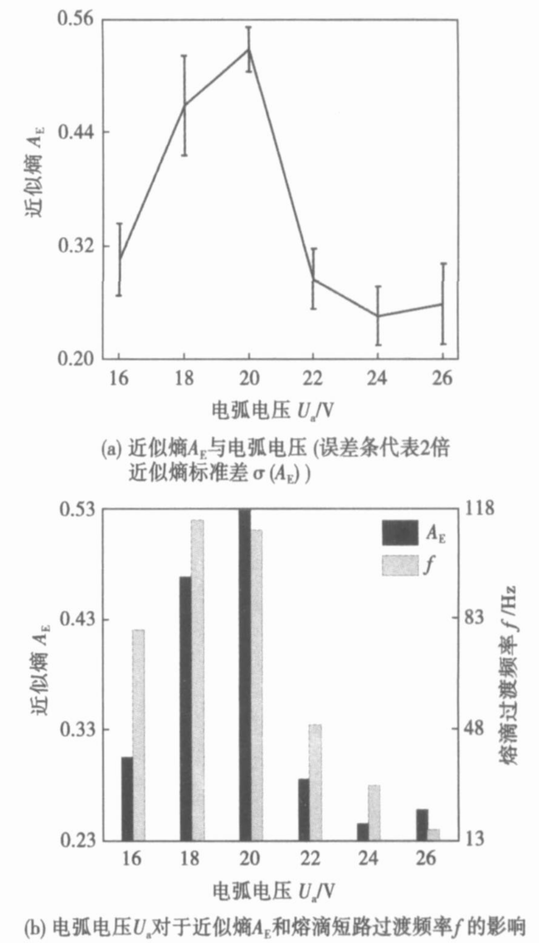

图 1 在不同电弧电压下，基于 120 000点焊接电流时间序列电弧电压 对于近似熵和熔滴短路过渡频率的影响

Fig. 1 Effects of U_a on A_E and f for welding current time series of length $N=120\ 000$ at different arc voltages U_a

熔化和固体顶丝，并时常伴随熄弧和飞溅产生，由于热输入不足，直接导致焊趾未熔合，焊缝产生裂纹和气孔. 另一方面，当 U_a≥22 V以上时，焊接过程也越来越不稳定. 通常高的电弧电压意味着大的电弧弧长. 当电弧弧长太大而与焊接电流不再匹配时，焊丝末端熔滴逐渐熔化并变得越来越大，并在焊丝末端作无规律地晃动. 随后，在电磁力、重力、等离子弧力和表面张力的综合作用下，熔滴脱离焊丝末端飞入熔池，但这往往不是沿着而是偏离焊丝轴线方向，所以熔滴是以大滴自由排斥过渡而非短路过渡的方式落入熔池，结果导致熔合不足和大量金属飞溅. 而且 U_a太高时，熔滴过渡以瞬时短路为主，而正常短路急剧减少，因此极易形成不良焊缝，产生气孔、咬边和未焊透以及焊缝余高过大，当然在这种情况下电弧飘移不定，焊接过程波动剧烈. 事实上，短路过渡 CO_2气体保护电弧焊电弧电压 U_a的适宜范围比较窄，通常约为 ±0.5 ~1.5 V. 当电弧电压

U_a合适时, 电弧发出轻快、均匀的噗噗声. 当弧压过低时, 声音不连续, 甚至出现固体短路和强烈飞溅; 而弧压过高时, 焊丝末端产生较大的球状熔滴, 电弧声不连续, f下降, 短路持续时间减少, 直至转变为以自由飞落形式过渡.

由物理试验和数值计算结果可知, 当 U_a从 16 V逐渐上升至 18 V时, 焊接过程也由不稳定状态过渡到稳定状态, A_E从 0.305 0上升至 0.468 7, f也由 79 Hz上升至 114 Hz; 当 18 V ≤ U_a ≤ 20 V时, 焊接过程平稳, 焊缝质量较好, A_E达到最大值 0.528 5, f也达到最大值 114 Hz左右; 当 U_a从 20 V上升至 26 V时, 焊接过程逐渐失稳, 焊缝质量变差, A_E则从 0.528 5下降至 0.258 0, 而 f则由峰值 114 Hz下降至最小值 16 Hz.

因此在整个 U_a的试验范围内, A_E及 f与焊接过程的稳定性变化趋势完全一致, 即 A_E, f都清晰表征了焊接过程的稳定性的动态变化, 从图 1可明显看出它们在量化焊接过程稳定性方面的作用相同.

3.2　不同气体流量下的近似熵 A_E分析

气体流量 q分别设置为 4, 6, 8, 10, 12, 14, 16和 18 L/min, U_a=20 V, 其它参数如 3.1节所述. 表 2列出了不同气体流量下 $\langle A_E \rangle$、$\sigma(A_E)$及 f的计算结果, 图 2a, b分别表明了 A_E随 q的变化和 q对于 A_E和 f的影响.

表 2　不同气体流量下近似熵均值 $\langle A_E \rangle$及标准差 $\sigma(A_E)$和熔滴过渡频率 f

Table 2　Mean $\langle A_E \rangle$ and its standard deviation $\sigma(A_E)$ and droplet transfer frequency f at different gas flow rates q

气体流量 q/(L·min⁻¹)	近似熵均值 $\langle A_E \rangle$	近似熵标准差 $\sigma(A_E)$	熔滴过渡频率 f/Hz
4	0.432 1	0.065 7	106
6	0.469 9	0.055 2	113
8	0.481 1	0.026 3	108
10	0.528 5	0.023 0	111
12	0.484 6	0.023 7	107
14	0.462 9	0.056 3	104
16	0.459 6	0.036 0	103
18	0.451 0	0.038 1	104

由物理试验和数值计算可知, 当 q从 4 L/min上升至 10 L/min时, 焊接过程逐渐从不稳定状态进入到稳定状态, A_E也从 0.432 1上升至 0.528 5, 然而 f处于 110 Hz左右, 变化不大; 当 q为 10 L/min时, 焊接过程平稳, 焊缝质量较好, 此时 A_E取得最大值 0.528 5, f为 111 Hz; 当 q从 10 L/min上升至 18 L/min以上时, 焊接过程又逐渐失稳, 焊缝质量变差, A_E则从 0.528 5下降至 0.451 0, 而 f仍旧保持在 110 Hz左右.

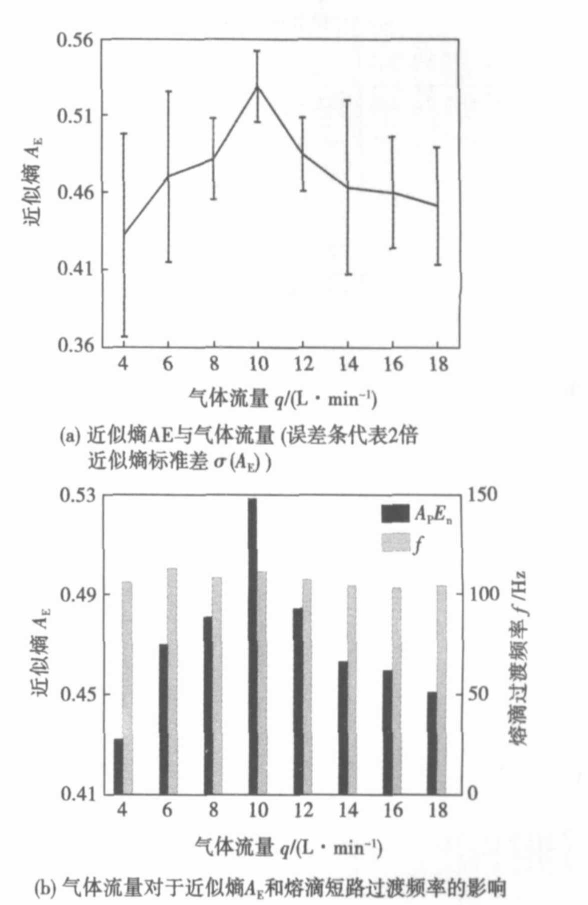

图 2　在不同气体流量下, 基于 120 000点焊接电流时间序列, 气体流量对于近似熵 A_E和熔滴短路过渡频率 f的影响

Fig. 2　Effects of q on A_E and f for welding current time series of length N=120 000 at different gas flow rates q

可见在整个 q的试验范围内, A_E与焊接过程的稳定性变化趋势完全一致, 而 f变化不大, 所以在改变 q的情况下 A_E清晰刻画了焊接过程稳定性的动态变化, 而 f显然不能够作为焊接过程稳定性的判断指标.

3.3　不同焊接速度下的近似熵 A_E分析

焊接速度 V_w分别设置为 21, 24, 27, 30, 33, 36, 39和 42 cm/min, U_a=20 V, 其它参数如 3.1节所述. 表 3是不同 V_w下 $\langle A_E \rangle$、$\sigma(A_E)$及 f的计算结果. 当 V_w从 21 cm/min上升至 42 cm/min时, 焊接过程逐渐从非稳态过渡到稳态 (30 cm/min ≤ V_w ≤ 33 cm/min), 随后又逐渐失稳, 由表 3显见 f对于 V_w所导致的稳定性动态变化不敏感, 而 A_E仍能作为焊接过程稳定性的鉴别指标.

表 3 不同焊接速度下近似熵均值及标准差和熔滴过渡频率

Table 3 Mean $<A_E>$ and its standard deviation $\sigma(A_E)$ and droplet transfer frequency f at different welding speeds v_w

焊接速度 v_w/(cm·min^{-1})	近似熵均值 $<A_E>$	近似熵标准差 $\sigma(A_E)$	熔滴过渡频率 f/Hz
21	0.457 8	0.031 0	103
24	0.452 8	0.033 5	105
27	0.475 0	0.027 9	103
30	0.528 5	0.023 0	111
33	0.499 4	0.020 8	110
36	0.474 2	0.060 4	112
39	0.465 9	0.054 6	110
42	0.461 3	0.068 9	109

4 结 论

(1) 物理试验和数值分析证明在改变 U_a 的条件下, A_E越大, f越高, 焊接过程越稳定.

(2) 在分别改变 φ和 v_w 的情况下, A_E仍与焊接过程稳定性成正相关关系, 但 f变化甚微, 难以反映焊接过程稳定性的动态变化, 因此 A_E比 f更全面准确刻画了 CO_2短路过渡过程稳定性的动态变化, 用于定量表征焊接系统的稳定性时优于 f.

参考文献:

[1] Pincus S M. Approximate entropy as a measure of system complexity[C] // Proceedings of the National Academy Sciences of the United States of America. Melville NY, 1991: 2297—2301.

[2] Pincus S M. Approximate entropy (AE) as a complexity measure [J]. Chaos, 1995, 5(1): 110—117.

[3] 殷树言. 气体保护焊工艺基础[M]. 1版. 北京: 机械工业出版社, 2007.

作者简介: 向远鹏, 男, 1971年出生, 博士, 讲师. 主要从事电力电子装置与电能变换技术的科研和教学工作. 发表论文 8篇.
Email: xiangyp519@qq.com

[上接第 20页]

低的界面反应能, 表明环己烯 POSS与锡的各主要晶面都有良好的结合性能, 但在其 (110)面上结合性能最好.

(2) Sn-Ag-Cu合金焊点中, 环己烯 POSS与合金表面的界面反应能高于纯锡表面的界面反应能, 表明银和铜影响了环己烯 POSS与锡的结合性能, 但结合性能依然较好.

(3) 结果对于理解 POSS对焊点的增强作用以及应用 POSS来开发焊料增强剂具有实际意义.

参考文献:

[1] Mavoori H, Jin S. New creep-resistant low melting point solders with ultrafine oxide dispersions[J]. Journal of Electronic Materials, 1998, 27(11): 1216—1222.

[2] Chen C M, Chen S W. Electromigration effect upon the Sn-0.7 wt% Cu/Ni and Sn-3.5 wt% Ag/Ni interfacial reactions[J]. Journal of Applied Physics, 2001, 90(3): 1208—1214.

[3] Schwab J J, Lichtenhan J D. Polyhedral oligomeric silsesquioxane (POSS)-based polymers[J]. Applied Organometallic Chemistry, 1998, 12(10—11): 707—713.

[4] Li G Z, Wang L, Toghiani H, et al. Viscoelastic and mechanical properties of vinyl ester (VE)/multifunctional polyhedral oligomeric silsesquioxane (POSS) nanocomposites and multifunctional POSS-styrene copolymers[J]. Polymer, 2002, 43(15): 4167—4176.

[5] Xu H Y, Kuo S W, Chang F C. Significant glass transition temperature increase based on polyhedral oligomeric silsequioxane (POSS) copolymer through hydrogen bonding[J]. Polymer Bulletin, 2002, 48(6): 469—474.

[6] Andre L, Subramanian K N. Development of nano-composite lead-free electronic solders[J]. Journal of Electronic Materials, 2005, 34(11): 1399—1407.

[7] Sun H. Ab initio calculations and force field development for computer simulation of polysilanes[J]. Macromolecules, 1995, 28(3): 701—712.

[8] Nocedal J. Updating quasi-newton matrices with limited storage [J]. Mathematics of Computation, 1980, 35: 773—782.

[9] Hoover W G. Constant pressure equation of motion[J]. Physics Review A, 1986, 34(3): 2499—2503.

[10] Nose S. A molecular dynamics method for simulations in the canonical ensemble[J]. Molecular Physics, 1984, 52(2): 255—268.

[11] Bicerano J. Prediction of polymer properties[M]. New York: Marcel Dekker Inc, 1993.

[12] Prathab B, Subramanian V, Aminabhavi T M. Molecular dynamics simulations to investigate polymer-polymer and polymer-metal oxide interactions[J]. Polymer, 2007, 4: 409—416.

[13] Kim K S, Huh S H, Suganuma K. Effects of intermetallic compounds on properties of Sn-Ag-Cu lead-free soldered joints[J]. Journal of Alloys and Compounds, 2003, 352(1—2): 226—236.

[14] Chun Y, Hao L. First principles calculations of the effects of Cu and Ag additions on the electromigration of Sn-based solder[J]. Journal of Applied Physics, 2007, 102(5): 1—4.

作者简介: 曾凡林, 男, 1978年出生, 工学博士, 讲师. 主要从事纳米复合材料力学、微纳米力学方面的科研和教学工作. 发表论文 20余篇.
Email: zengfanlin@hit.edu.cn

POSS on the (100), (110) and (001) planes of the lead free solder joints β-Sn and on the surface of the Sn-Ag-Cu alloy were performed via the molecular dynamics (MD) simulations. The cohesive energies were also obtained. The results show that the cyclohexenyl-POSS can be easily absorbed on the main crystal planes of β-Sn. But the cohesive energy on (110) plane is the lowest, thus the cyclohexenyl-POSS will be absorbed on the (110) plane most likely. Adding the silver (Ag) and the copper (Cu) into β-Sn to form the Sn-Ag-Cu alloy raises the cohesive energies of cyclohexenyl-POSS on the alloy surfaces and generate the unfavorable absorbing effect. But the cyclohexenyl-POSS can also be easily absorbed on the surfaces. Moreover, the solubility parameter of the cyclohexenyl-POSS was computed from the MD simulations.

Key words: cyclohexenyl-POSS; lead free solder joints; cohesive energy; solubility parameter

Effects of approximate entropy and droplet transfer frequency on process stability of CO_2 short-circuiting welding XIANG Yuanpeng, CAO Biao (1. School of Mechatronics Engineering, University of Electronics and Science Technology of China, Chengdu 611731, China; 2. School of Mechanical and Automotive Engineering, South China University of Technology, Guangzhou 510641, China). p21—24

Abstract: Based on the experimental time series of welding current produced by CO_2 welding with short-circuiting transfer under different arc voltages, gas flow rates and welding speeds, the approximate entropy of the welding current has been numerically evaluated by the implementation of Pincus' s algorithm. The different effects of approximate entropy and droplet short-circuiting transfer frequency on the welding process stability are also analyzed. Experiments and numerical analysis demonstrate that approximate entropy reaches larger values when the welding processes approach more steady states under the condition of the three above-mentioned process experiments. The variation trend of the droplet short-circuiting transfer frequency is not always consistent with that of welding process stability. So approximate entropy characterizes the welding process stability more accurate than the droplet transfer frequency.

Key words: CO_2 short-circuitong weld; approximate entropy; droplet trarsfer frequency

RSW fuzzy artificial neural network control method based on variable universe YUAN Qingke, SHI Yaping, ZHANG Mingtian, FENG Sang (College of Mechanical & Electrical Engineering, Guangdong University of Technology, Guangzhou 510006, China). p25—28, 32

Abstract: In order to enhance the control precision and welding quality of resistance spot welding (RSW), according to the RSW control characteristics, it put forward the RSW fuzzy artificial neural network (FANN) control method based on variable universe by integrating the variable universe technology and FANN. The network structure of FANN was designed and the process of neural computation dealing with the fuzzy, the fuzzy rules and the solution of fuzzy was analyzed. And the method of how to fix on the extension-contraction factors of input and output universe was researched. Then a kind of FANN controller of RSW with the variable universe was developped, being applied to a kind of spot welding experiments to study and analyze. The results prove the FANN control method is better than other fuzzy control methods.

Key words: fuzzy control; spot welding; artificial neural network; variable universe; extension-contraction factors

Influence of electrochemical reaction on oxygen pick-up for droplet metal in direct current welding LI Xiaoquan, CHU Yajie, YANG Zonghui (School of Material Engineering, Nanjing Institute of Technology, Nanjing 211167, China). p29—32

Abstract: On the basis of oxygen pick-up dynamic analysis in droplet metal, a series of self-made agglomerative fluxes with different basicity indexes were used, by the droplet metal on water cooled copper with no weld pool adopting direct current submerged arc welding, so as to obtain some quality and geometric messages contained in droplet metal for its oxygen pick-up analysis resulted from electrochemical reaction. The results show that, with the increase of slag basicity index, eletrochemical reaction occurring at the interface of slag-metal would be more obvious, and so is the amount of oxygen gaining from electrochemical reactuon. For $CaO-Al_2O_3-SiO_2$ slag in this study, the extend of oxygen gaining from electrochemical reaction can be almost equal to that from thermo-chemical, therefore it is an in-negligible oxygen induced factor in formulating direct current welding technology or developping high basic index welding consumables.

Key words: electrochemical reaction; direct current welding; droplet metal; induced oxygen; basicity index

M_7C_3-type carbide and abrasion resistance of Fe-C-Cr-V high chromium hardfacing alloys GONG Jianxun, XIAO Yifeng, ZHANG Qinghui, MA Min (1. School of Mechanical Engineering, Xiangtan University, Xiangtan 411105, Hunan, China; 2. Faculty of Material and Photoelectronic Physics, Xiangtan University, Xiangtan 411105, Hunan, China). p33—36

Abstract: High chromium hardfacing alloys containing 0.9-3.0% C, 15-20% Cr, 2.0-3.0% V (wt%) were deposited by flux-cored wire submerged arc welding (SAW). The microstructure and carbide morphology were investigated by optical microscopy (OP), scanning electron microscopy (SEM) and X-ray diffraction (XRD). The microstructure consists of martensite, ferrite and austenite, carbide such as primary M_7C_3 ((Fe, Cr)$_3$C and TiC etc. Orientational M_7C_3-type carbide grains distributing in the plane vertical to the hardfacing surface were obtained by the optimization of flux-cored wire and welding speed. The analysis of energy dispersive spectrometer (EDS) indicated that M_7C_3 type carbide was (Fe, Cr, V)$_7C_3$. In addition, the effects of carbon content on hardness and wear properties were evaluated. Experimental results demonstrated that the abrasion re-